JVI Journals.ASM.org

Measles Virus Infection of Epithelial Cells in the Macaque Upper Respiratory Tract Is Mediated by Subepithelial Immune Cells

Martin Ludlow,[a] Ken Lemon,[b] Rory D. de Vries,[c] Stephen McQuaid,[b,d] Emma L. Millar,[c] Geert van Amerongen,[c] Selma Yüksel,[c] R. Joyce Verburgh,[c] Albert D. M. E. Osterhaus,[c] Rik L. de Swart,[c] W. Paul Duprex[a,b]

Department of Microbiology, Boston University School of Medicine, Boston, Massachusetts, USA[a]; School of Medicine, Dentistry and Biomedical Sciences, The Queen's University of Belfast, Belfast, Northern Ireland, United Kingdom[b]; Department Viroscience, Erasmus MC, Rotterdam, The Netherlands[c]; Tissue Pathology Laboratories, Belfast Health and Social Care Trust, Belfast, Northern Ireland[d]

Measles virus (MV), one of the most contagious viruses infecting humans, causes a systemic infection leading to fever, immune suppression, and a characteristic maculopapular rash. However, the specific mechanism or mechanisms responsible for the spread of MV into the respiratory epithelium in the late stages of the disease are unknown. Here we show the crucial role of PVRL4 in mediating the spread of MV from immune to epithelial cells by generating a PVRL4 "blind" recombinant wild-type MV and developing a novel *in vitro* coculture model of B cells with primary differentiated normal human bronchial epithelial cells. We utilized the macaque model of measles to analyze virus distribution in the respiratory tract prior to and at the peak of MV replication. Expression of PVRL4 was widespread in both the lower and upper respiratory tract (URT) of macaques, indicating MV transmission can be facilitated by more than only epithelial cells of the trachea. Analysis of tissues collected at early time points after experimental MV infection demonstrated the presence of MV-infected lymphoid and myeloid cells contacting respiratory tract epithelium in the absence of infected epithelial cells, suggesting that these immune cells seed the infection *in vivo*. Thereafter, lateral cell-to-cell spread of MV led to the formation of large foci of infected cells in the trachea and high levels of MV infection in the URT, particularly in the nasal cavity. These novel findings have important implications for our understanding of the high transmissibility of measles.

Measles virus (MV), the prototype morbillivirus of the family *Paramyxoviridae*, remains a major cause of morbidity and mortality in the developing world and is highly transmissible (1). Recent drops in vaccination rates in Europe have resulted in large-scale outbreaks of measles in a number of countries, with 30,567 cases, 8 deaths, and 27 cases of acute encephalitis reported in 2011 (2). It is estimated that global measles mortality is still above 100,000 cases per year (3). While the epidemiology of measles has been extensively studied and virus transmission is known to take place via the respiratory route, a paucity of data exists on the mechanisms by which MV spreads from person to person.

In contrast to other paramyxoviruses, such as human respiratory syncytial virus (HRSV) and human metapneumovirus, which predominantly infect ciliated epithelial cells in the respiratory tract, MV primarily targets myeloid and lymphoid cells and causes a systemic disease. Spread of virus to respiratory tract tissues following viremia is thought to be a key for MV transmission. Studies showing that the apical side of ciliated epithelial cells is refractory to MV infection showed that these cells are not primary target cells when MV enters the respiratory tract (4, 5). However, the susceptibility of the basolateral side of epithelial cells to MV infection has led to the proposal that MV crosses the airway epithelium by directly infecting epithelial cells in the late stages of the disease (6). Virus budding from the apical cell surface would then enable efficient transmission of virus via respiratory aerosols. The recent identification of PVRL4 (nectin 4) as a cellular receptor for MV on some epithelial cell-lines (7) and subsequent confirmation and extension of this finding to primary differentiated epithelial cells grown on an air-liquid interface (ALI) (8) provided a mechanism through which MV infection of epithelial cells may occur *in vivo*.

We have previously investigated the early and viremic phases of measles in the macaque model, showing that alveolar macrophages and dendritic cells acted as early targets of MV infection (9–11). In addition, we demonstrated a prominent role for $CD150^+$ lymphocytes and myeloid cells in facilitating the spread of virus to lymphoid tissues throughout the body (9, 10). Moreover, we demonstrated that infection and subsequent depletion of memory T lymphocytes and follicular B lymphocytes may largely explain measles immune suppression (12). In the present study, we have examined the mechanism(s) by which MV crosses the epithelium to emerge into the respiratory tract at and shortly after the peak of infection. We report a critical role for PVRL4 in mediating virus spread from immune to epithelial cells through a novel B-lymphocyte/epithelial cell model and show high levels of epithelial cell infection in the upper respiratory tract (URT), a finding which enhances our understanding of MV transmission.

MATERIALS AND METHODS

Cells and viruses. Two recombinant wild-type MV strains expressing enhanced green fluorescent protein (EGFP) from an additional transcription unit (ATU), rMV^{IC323}EGFP and rMV^{KS}EGFP, validated in the macaque model previously (9, 10, 13), were used in this study to facilitate sensitive macroscopic and microscopic detection of MV infection. An additional virus was generated that does not bind PVRL4 (see below). Virus stocks were generated in an Epstein-Barr virus-transformed human B-lymphoblastic cell line (B-LCL) and were tested to ensure the absence of *Mycoplasma* species prior to use. Virus titers were obtained by endpoint

Received 22 November 2012 **Accepted** 22 January 2013
Published ahead of print 30 January 2013
Address correspondence to Rik L. de Swart, r.deswart@erasmusmc.nl.

doi:10.1128/JVI.03258-12

titration in Vero cells stably expressing human or canine CD150 (Vero-hCD150 and Vero-cCD150, respectively) and were expressed as 50% tissue culture infectious doses ($TCID_{50}$)/ml using the formula of Reed and Muench (14).

Generation of an rMV unable to bind PVRL4. Given that we have recently generated a range of viruses with the ATU in alternative positions in the genome, we extended the name of the virus to "rMV^{KS}EGFP(1)" to reflect these developments. The number in parentheses refers to the genomic position of the ATU. Site-directed mutagenesis was used to introduce two mutations (P497S and P543A) into the open reading frame (ORF) of the hemagglutinin (H) gene in the full-length antigenomic plasmid pMV^{KS}EGFP(1) to generate pMV^{KS}EGFP(1)PVRL4^{-}. This was transfected into Vero-cCD150 cells, previously infected with a recombinant fowlpox virus expressing T7 polymerase (FP-T7), along with helper plasmids encoding the nucleocapsid (N), phospho (P)-, and large (L) proteins of MV^{KS}. The amounts of each plasmid used are as follows: pMV^{KS}EGFP(1)PVRL4^{-}, 10 μg; N, 1 μg; P, 0.6 μg; and L, 0.4 μg. Syncytia were observed 4 to 6 days posttransfection (d.p.t.), and EGFP expression was confirmed by UV microscopy. Cells were scraped into the medium and subjected to one freeze-thaw cycle. Clarified supernatant was used to infect B-LCL. Following two passages in B-LCL, viral titers were determined on Vero-cCD150 or Vero-hCD150 cells and expressed in $TCID_{50}$/ml.

Differentiation of NHBE cells. Normal human bronchial epithelial (NHBE) cells (Lonza, Inc., Walkersville, MD) were differentiated (dNHBE) on type I collagen- and fibronectin-coated 6.5-mm Transwell inserts with a 0.4-μm pore size (Corning, Lowell, MA) using an air-liquid interface as described previously (15). Transepithelial electrical resistance was measured using an STX3 electrode and EVOM meter device (World Precision Instruments) with Transwells used for experiments displaying $>800\ \Omega \times cm^2$. Cells were monitored using a DM IRBE UV microscope (Leica Microsystems), and images were collected using a Leica DM600B microscope equipped with a Leica DFC350 FX digital camera and processed using Leica FW4000 software.

Animal study design. Cells and tissues were collected from cynomolgus macaques ($n = 35$) and rhesus macaques ($n = 5$) that were infected with rMV^{IC323}EGFP or rMV^{KS}EGFP and euthanized at 2 ($n = 3$), 3 ($n = 3$), 4 ($n = 3$), 5 ($n = 4$), 7 ($n = 9$), 9 ($n = 8$), 11 ($n = 6$), 13 ($n = 2$), or 15 ($n = 2$) days postinfection (d.p.i.) as reported previously (12). Animals were housed and experiments were conducted in compliance with European guidelines (EU Directive on Animal Testing 86/609/EEC; http://ec.europa.eu/food/fs/aw/aw_legislation/scientific/86-609-eec_en.pdf) and Dutch legislation (Experiments on Animals Act, 1997; http://wetten.overheid.nl/BWBR0003081). The protocols were approved by an independent animal experimentation ethical review committee, and animal welfare was observed on a daily basis. Animal handling was performed under light anesthesia using ketamine and medetomidine. After handling, atipamezole was administered to antagonize the effect of medetomidine.

Necropsies. Animals were euthanized by exsanguination under ketamine/medetomidine anesthesia, and macroscopic foci containing EGFP were visualized and photographed as described previously (10, 13). Samples collected for direct detection of EGFP were collected in freshly prepared 4% (wt/vol) paraformaldehyde (PFA) in phosphate-buffered saline (PBS), while samples required for histological, immunohistochemical, or immunocytochemical analysis were collected in buffered formalin and subsequently blocked in paraffin. Representative blocks from lung and multiple transverse cut blocks from trachea and primary bronchus, nasal septum, and nasal concha, were analyzed.

Immunohistochemical and immunofluorescence analysis of formalin-fixed tissues. All formalin-fixed sections were deparaffinized, antigen retrieval was performed, and MV-infected cells were detected as described previously (10) using polyclonal rabbit antibodies to EGFP (Invitrogen) or anti-measles N protein (Novus Biologicals), while PVRL4 present in adherens cell junctions in epithelia was detected using a polyclonal rabbit antibody (Sigma). An Envision peroxidase system with 3,3′-diaminobenzidine (DAB) (Dako) as the substrate was used to detect antigen binding sites. Following assessment of histology and virus immunopathology in respiratory tract tissues, blocks were selected for dual-labeling immunofluorescence performed using polyclonal rabbit antibodies to EGFP (Invitrogen), polyclonal rabbit and monoclonal mouse antibodies to measles N protein together with monoclonal mouse antibodies to the myeloid cell marker CD11c (Novocastra clone no. 5D11), T-lymphocyte marker CD3 (Dako, clone F7.2.38), B-lymphocyte marker CD20 (Dako, clone L26), cell proliferation marker Ki-67 (Dako, clone MIB-1), and an epithelial cytokeratin cell marker (Dako, clone AE1/AE3) or a polyclonal rabbit antibody to PVRL4 (Sigma). Antigen binding sites were detected using anti-mouse rabbit Alexa 488-conjugated and anti-mouse rabbit and human Alexa 568-conjugated antibodies. Following washes to remove unbound antibody, sections were mounted on glass slides using DAPI (4′,6-diamidino-2-phenylindole) HardSet mounting medium (Vector). Selected hematoxylin-and-eosin (H&E)-stained or immunohistochemically stained sections were digitally scanned at high resolution and imaged using PathXL software package (i-Path Diagnostics, Ltd.). Images from immunofluorescence-stained slides were obtained using a fluorescent imaging microscope (Leica Microsystems).

RESULTS

Development of an *in vitro* coculture model of MV spread from immune cells to respiratory epithelial cells to assess cell-to-cell spread. The role of MV-infected immune cells in seeding the infection within respiratory tract epithelial cells was investigated by establishing an *in vitro* coculture model using human B-LCL and primary dNHBE cells cultured on an ALI. This allowed virus spread to be monitored over time, first from rMV-infected B-LCL to epithelial cells and second from these infected dNHBE cells to neighboring dNHBE cells. B-LCL (10^4) were infected with rMV^{KS}EGFP(1) at a multiplicity of infection (MOI) of 1 for 24 h. Prior to use in overlay experiments, the rMV-infected B-LCL were rinsed in Dulbecco's phosphate-buffered saline to remove any cell-free virus. Absence of residual virus was confirmed by adding the final washing to Vero-hCD150 cells and incubating the cells for 7 days. MV-infected cells were either overlaid onto the apical surface of intact dNHBE ALI cultures or onto cultures in which the basolateral surface had been exposed by wounding the cells using a pipette tip to scratch the surface of the transwell (Fig. 1A; phase-contrast photomicrograph). Epithelial cells never became infected when rMV-infected B-LCL were overlaid onto the apical surface of the ALI culture (data not shown). Single fluorescent rMV^{KS}EGFP(1)-infected B-LCL adhered to the scratched surface shortly after overlay (Fig. 1A; fluorescence photomicrograph). Spreading of rMV^{KS}EGFP(1) into epithelial cells occurred from 12 h postoverlay (h.p.o.), and small foci of approximately 10 to 15 MV-infected epithelial cells were readily distinguished from adjacent fluorescent B-LCL at 24 h.p.o. (Fig. 1A, arrows). Subsequent MV cell-to-cell spread resulted in progressively larger foci of >100 infected cells at 48 and 72 h.p.o. This demonstrated the importance of cell-to-cell spread in initiating the infection of primary epithelial cells.

A previous study using the wild-type IC323 strain of MV (16) identified residues in the H glycoprotein that are critical for infection of epithelial cells (6). Mutation of amino acids P497F and Y543A abolished entry into epithelial cell lines and did not affect the ability of the virus to use CD150 as a receptor. To prove the generality of this observation, equivalent mutations were introduced into the full-length plasmid pMV^{KS}EGFP (9) to generate pMV^{KS}EGFP(1)PVRL4^{-} (Fig. 1B) and rMV^{KS}EGFP(1)PVRL4^{-} was recovered in Vero-cCD150 cells and passaged twice in B-

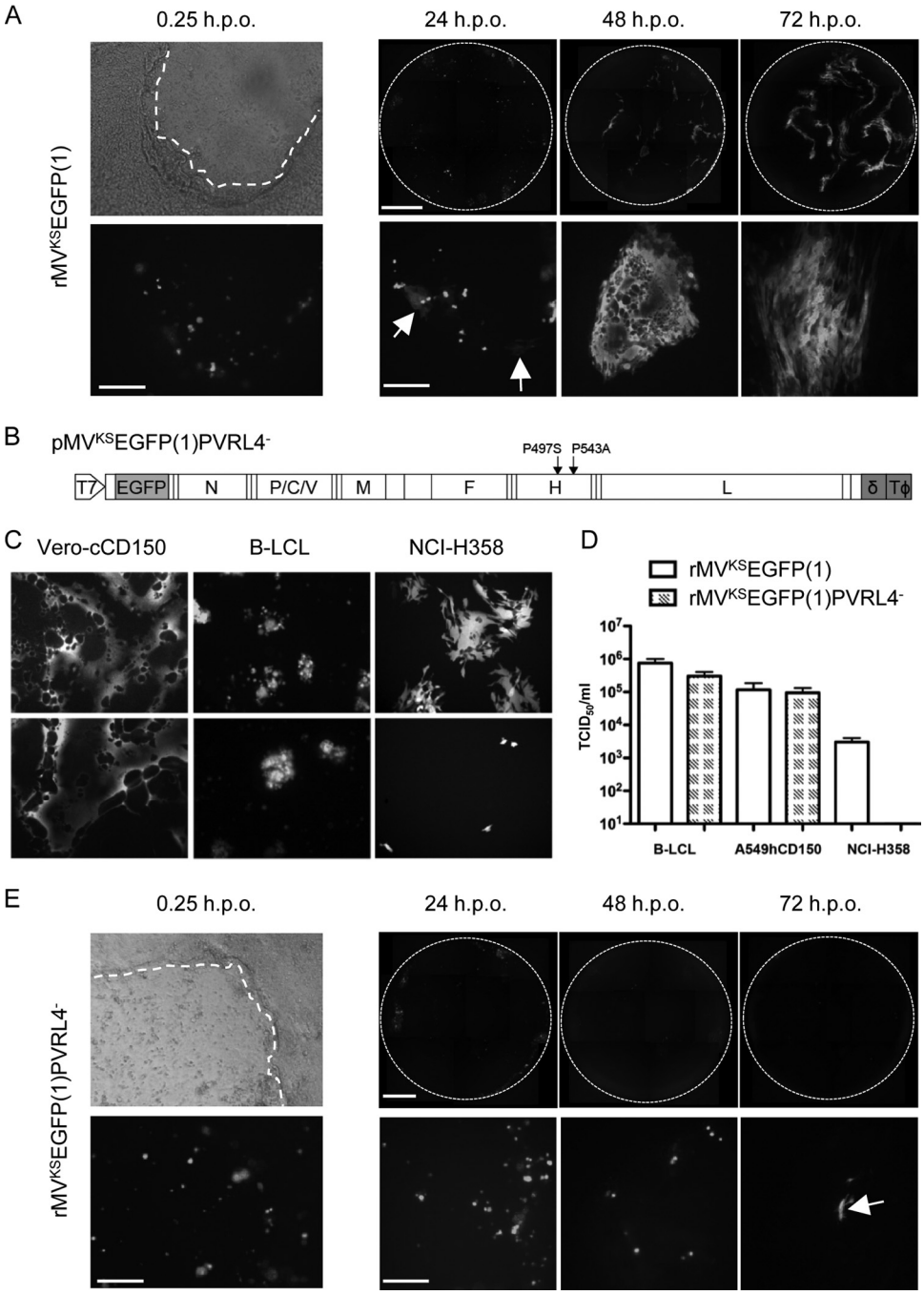

FIG 1 rMV^{KS}EGFP(1)PVRL4^{-} fails to spread from infected B-cells to adjacent epithelial cells. (A and E) Time course of infection following overlay of rMV^{KS}EGFP(1)-infected B-LCL onto scratched dNHBE cells grown on ALI. Phase-contrast and fluorescence photomicrographs of the same field of view 15 min postoverlay of infected B-LCL are shown in the left panels; fluorescent images of the entire Transwells at 24, 48, and 72 h.p.o. are shown in the right panels (top) with representative higher-magnification images shown on the bottom. A dashed white line indicates the approximate location of the wound site in the phase-contrast photomicrographs. (A) rMV^{KS}EGFP(1) infection of epithelial cells occurred 24 h.p.o. (arrows), and virus cell-to-cell spread increased at 48 and 72 h.p.o. (E) rMV^{KS}EGFP(1)PVRL4^{-}-infected B-LCL are visible at 0, 24 and 48 h.p.o., with isolated examples of limited epithelial cell infection present at 72 h.p.o. (arrow). Bars: 0 h.p.o., 200 μm; 24 to 72 h.p.o., top row, 800 μm; bottom row, 200 μm. (B) Schematic representation of the full-length antigenomic plasmid with site-directed mutations in the H gene used to recover MV^{KS}EGFP(1)PVRL4^{-} showing the T7 promoter, the position of the ATU containing the EGFP ORF, the hepatitis δ ribozyme (δ), and T7 RNA polymerase terminator sequences (TΦ). (C) Infection of Vero-cCD150, B-LCL, and NCI-H358 cell lines with rMV^{KS}EGFP(1) (upper panels) and MV^{KS}EGFP(1)PVRL4^{-} (lower panels). (D) Quantification of supernatant virus released from rMV^{KS}EGFP(1) and rMV^{KS}EGFP(1)PVRL4^{-} virus-infected B-LCL, A549-hCD150, and NCI-H358 cells.

LCL. Reverse transcription (RT)-PCR and sequence analysis confirmed that the mutations were stably maintained upon virus passage (data not shown). The ability of rMV^{KS}EGFP(1) and rMV^{KS}EGFP(1)PVRL4^{-} to infect a range of cell lines was examined. Both viruses infected CD150-expressing cell lines Vero-cCD150 and B-LCL equivalently (Fig. 1C). The human epithelial cell line NCI-H358 (17) expresses PVRL4 (8), and numerous foci were present when these were infected with rMV^{KS}EGFP(1) (Fig. 1C). When NCI-H358 cells were infected with rMV^{KS}EGFP(1)PVRL4^{-}, only very small numbers of isolated fluorescent cells were detected and there was no cell-to-cell spread. In order to quantify the ability of B-LCL, an A549 cell line stably expressing human CD150 (A549-hCD150), and the NCI-H358 cell line to support infection, they were infected in triplicate with both viruses and supernatants were harvested at 2 d.p.i. (B-LCL and A549-hCD150) or 3 d.p.i. (NCI-H358). The titer of released virus was determined on Vero-cCD150 cells, and equivalent amounts of virus were obtained when the viruses were grown on CD150-expressing cell lines (Fig. 1D). NCI-H358 cells generated 100 times less rMV^{KS}EGFP(1) than CD150-expressing cells, and no progeny virus was recovered from rMV^{KS}EGFP(1)PVRL4^{-}-infected NCI-H358 cells.

Ubiquitous expression of PVRL4 on the surface of a cell does not reflect the *in vivo* situation in which the molecule is localized within the adherens junction. Furthermore, cell-associated rather than cell-free virus is the form in which the infectivity is transmitted from an immune to an epithelial cell, making the *in vitro* coculture model ideal for the study of this late-stage event in MV pathogenesis. B-LCL (10^4) were infected with rMV^{KS}EGFP(1)PVRL4^{-} and overlaid onto wounded dNHBE cells (Fig. 1E; phase-contrast photomicrograph) as described above. Although the MV^{KS}EGFP(1)PVRL4^{-}-infected B-LCL adhered to the scratch equivalently (Fig. 1E; fluorescent photomicrograph), the infectivity was not transferred to the epithelial cells. Small numbers of rMV^{KS}EGFP(1)PVRL4^{-}-infected B-LCL remained at 24 and 48 h.p.o. In rare instances, foci comprised of 2 or 3 infected epithelial cells apparently were observed at 72 h.p.o. (Fig. 1E, arrow).

PVRL4 is detected in epithelia in a large number of tissues from both the LRT and URT. Formalin-fixed and paraffin-embedded dNHBE cells were used to test a number of commercial antibodies to PVRL4. Upon identification of a polyclonal antibody that met our criteria for acceptable levels of background staining and a staining pattern consistent with our understanding of spatial PVRL4 expression as a component of the adherens junction within epithelia (Fig. 2A), this antibody was used to examine the PVRL4 distribution in a large number of respiratory tract tissues from uninfected and MV-infected macaques. Prior to use, the specificity of the antibody was verified and optimized by immunocytochemical staining of PVRL4 along the membrane of CHO-K1 cells transfected with a plasmid expressing human PVRL4, while negative staining was observed in cells transfected with an empty vector control plasmid (data not shown). High levels of PVRL4 expression were observed in the nonkeratinized stratified squamous epithelia of the tonsil, with strong PVRL4 expression observed around the cell membrane of epithelial cells (Fig. 2B). An analogous PVRL4 staining pattern was observed in focal areas of tongue epithelium (Fig. 2C). In contrast, a more irregular polarized staining pattern was observed in nasal concha epithelia in the URT and tracheal epithelia in the lower respiratory tract (LRT), in which PVRL4 was mainly detected along the basolateral surface of pseudostratified columnar epithelial cells (Fig. 2D and E). High levels of PVRL4 expression were also observed in the lung, especially in epithelial cells surrounding the lumen of the bronchi (Fig. 2F).

MV infection of respiratory tract tissues is widespread at the peak of MV infection. The spread of MV within respiratory tract tissues of macaques was examined at different time points postinfection with wild-type rMV strains expressing EGFP. This permitted targeted pathological assessment allowing the optimal selection and blocking of samples for formalin fixation, paraffin embedding, and microtome sectioning. Extensive EGFP fluorescence, indicative of MV infection, was visible throughout the respiratory tract at the peak of infection at 9 d.p.i. Foci of MV infection were visible in all lobes of the lung (Fig. 3A) and along the entire length of the trachea (Fig. 3B). Microscopic examination of the inner surface of intact trachea rings obtained from animals at the peak of infection revealed circular foci of MV-infected epithelial cells (Fig. 3C). These may arise via the lateral spread of virus within the epithelium following initial infection of an epithelial cell, akin to virus cell-to-cell spread *in vitro* (compare with Fig. 1A). Examination of transverse sections through the nose facilitated the detection of very large numbers of infected cells in the nasal concha and, even more extensively, in the adjacent nasal mucosa (Fig. 3D). Live cell confocal scanning laser microscopy of the unfixed, unprocessed nasal concha collected directly from infected animals at necropsy revealed irregularly shaped foci of morphologically identifiable infected epithelial cells on the surface of the tissue (Fig. 3E), illustrating the lateral spread of MV between epithelial cells once infection is established in the epithelium. Individual foci of infection were also detected in the epithelium of the nasal septum (data not shown). This mirrors what was modeled *in vitro* using B-LCL and dNHBE cells (Fig. 1A).

MV infection of epithelial cells occurs following contact with infected immune cells in respiratory tract epithelium. Respiratory tract tissue sections were examined at 7 d.p.i., 1 or 2 days prior to the peak of viremia, to assess how MV spreads into respiratory tract epithelial cells. While a low level of epithelial cell infection was observed in most respiratory tract tissues (data not shown), an observation we have previously reported at this time point (5, 10), immune cells were the predominant MV-infected cell lineage present in respiratory tract epithelia at this time point. Low levels of MV-infected immune cells were present in close proximity to tracheal epithelium, with leukocytes or cellular processes interdigitating into the epithelium from underlying infected myeloid cells spanning the basement membrane, providing a route of virus entry into epithelial cells (Fig. 4A and B). The absence of MV-infected epithelial cells at many of these sites at this time point suggests that infiltration of infected immune cells or alternatively infection of resident immune cells in respiratory tract epithelium is an inherent pathological feature of MV infection and is not occurring in response to MV infection of epithelial cells. Limited lateral spread of virus within the epithelium resulted in small foci of infected tracheal pseudostratified ciliated columnar epithelial cells by 9 d.p.i. (Fig. 4C). CD11c^{+} myeloid cells were present in the lamina propria beneath tracheal epithelium (Fig. 4D), with CD3^{+} T cells observed in close proximity to MV-infected epithelial cells (Fig. 4E). Uninfected and infected CD20^{+} B cells were present within bronchial epithelium, especially in areas overlying large aggregates of lymphoid tissue (Fig. 4F).

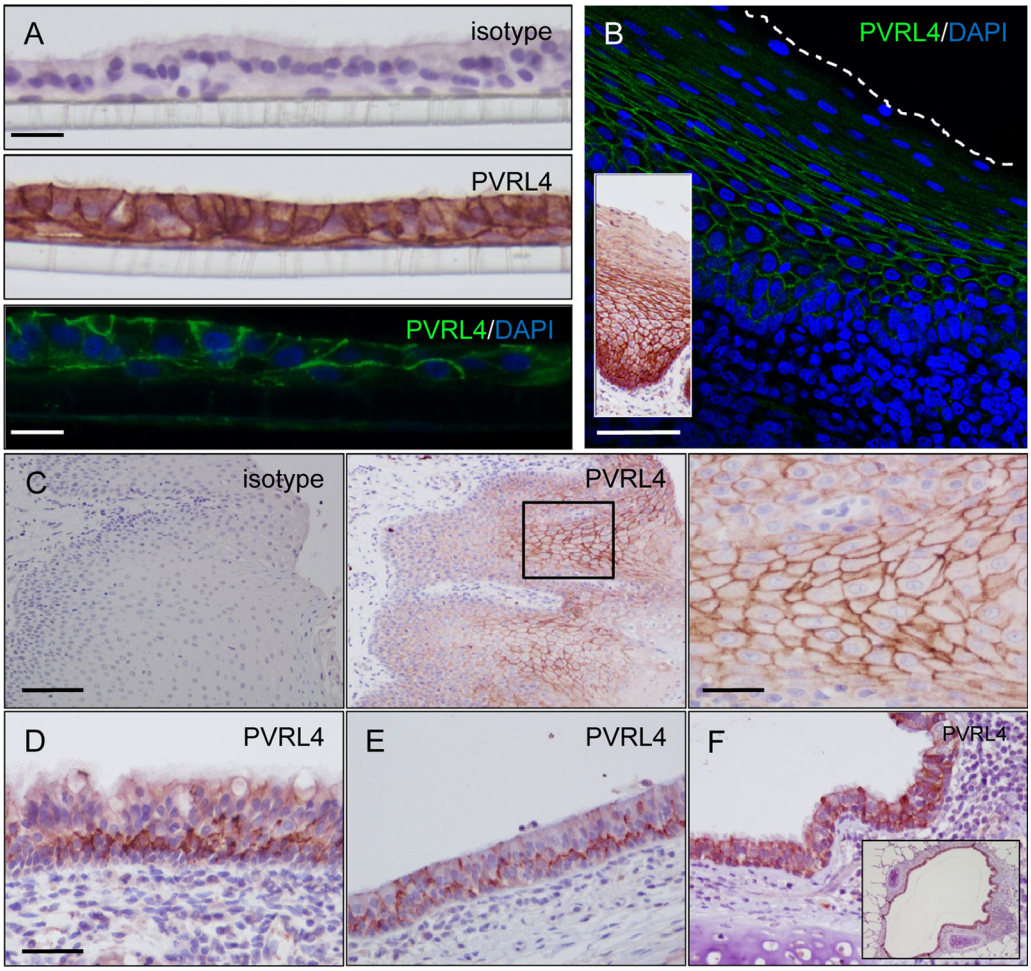

FIG 2 Localization of PVRL4 within primary epithelial cells and macaque respiratory tract epithelia. (A) dNHBE cells were grown on ALI, fixed in 4% (wt/vol) PFA, and paraffin embedded. Sections (7 μm) were cut, probed with an isotype antibody control, and H&E stained to show the multiple cell layers and cilia (top). PVRL4 localization was examined by using immunohistochemistry (middle, brown staining) and indirect immunofluorescence (bottom, green staining), with nuclei being counterstained by H&E or DAPI, respectively. PVRL4 was present along the basolateral surface of epithelial cells and at cell-to-cell junctions. Limited staining was observed along the basolateral surface of basal cells in direct contact with the plastic membrane on which the cells are cultured. Bars: top and middle, 50 μm; bottom, 30 μm. (B) Indirect immunofluorescence (main panel) staining of PVRL4 in formalin-fixed tissue sections taken from the tonsil of infected macaques at 9 d.p.i. PVRL4 is present around the entire surface of stratified squamous epithelial cells (green). Bar, 120 μm. (Inset) Immunohistochemical staining of PVRL4 showing an analogous staining pattern in the epithelium. (C) Immunohistochemical staining of PVRL4 (middle and right panels) in formalin-fixed tissue sections taken from the tongue with an isotype control (left panel) for comparison. PVRL4 is present around the entire cell membrane of squamous epithelial cells. Bars: left and middle, 160 μm; right, 40 μm. (D to F) PVRL4 was detected along the basolateral surface of pseudostratified ciliated epithelial cells in the nasal concha (D) and trachea (E) and at cell boundaries of bronchial epithelial cells in the lung (F). High levels of PVRL4 are present throughout the bronchial epithelium surrounding the lumen of the bronchus (inset). Bar (D to F), 80 μm.

Lateral cell-to-cell spread of MV is observed in both tracheal and nasopharynx epithelia. Spread of virus from immune cells resulted in MV infection of ciliated pseudostratified columnar epithelial cells. Dual labeling for MV N protein and cytokeratin showed accumulation of N protein underneath the apical membrane of MV-infected epithelial cells and an absence of infection in cytokeratin-positive cells present within lower layers of the epithelium (Fig. 5A). Further analysis of the differential susceptibility of tracheal epithelial cells to MV infection by dual labeling with EGFP and Ki-67, a marker of cellular proliferation, demonstrated that MV-negative epithelial cells present in basal cell layers of the epithelium stain positive for Ki-67 and thus represent a population of uninfected proliferating epithelial cells (Fig. 5B). Analysis of PVRL4 distribution showed that highest expression levels were present at the cell boundaries of basal tracheal epithelial cells, with no discernible concomitant downregulation of PVRL4 expression visible within large foci of MV-infected cells (Fig. 5C).

High levels of MV-infected cells were present in the nasal cavity of MV-infected macaques at the peak of infection (Fig. 3D), indicating a key role for nasal epithelium in MV transmission. Examination of a transverse section through the nasal concha revealed high levels of epithelial cell infection and epithelial damage due to shedding of these cells into the lumen (Fig. 5D). In the nasal mucosa, MV mainly infected ciliated pseudostratified columnar epithelial cells, with contiguous epithelial cell infection and exfoliation of MV-infected epithelial cells into the nasal cavity observed as characteristic features of the infection in the URT (Fig. 5E and F). In common with the distribution of MV-infected cells in tra-

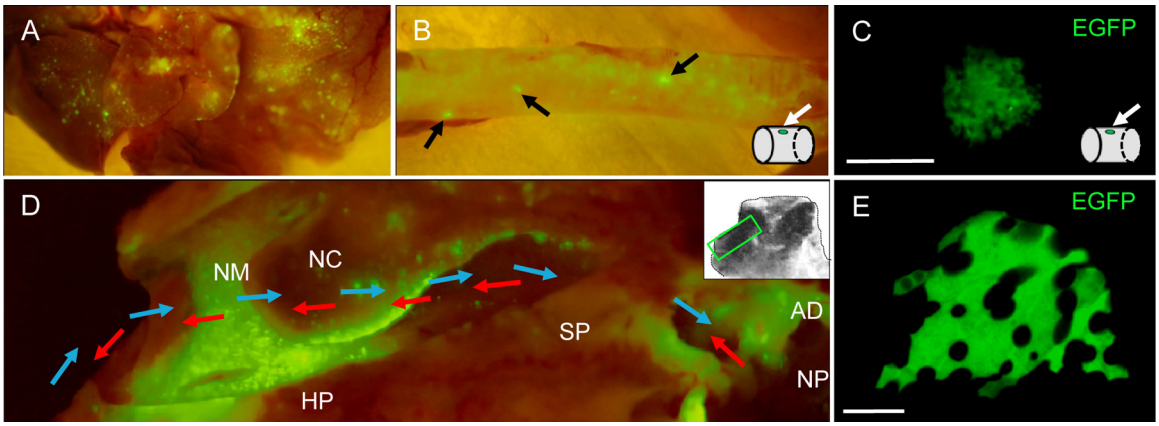

FIG 3 Detection of EGFP fluorescence in respiratory tract tissues from macaques infected with wild-type rMV. Tissues were examined macroscopically for MV infection at the peak of infection (9 to 11 d.p.i.). (A) All lobes of the lung contained foci of MV infection. (B) Small circular foci (arrows) were present along the trachea. A schematic diagram illustrates the presence of the circular EGFP-positive focus on the inside wall of the trachea. (C) Direct detection of a focus of MV-infected epithelial cells on the luminal surface of the trachea. No cell-to-cell fusion was observed within the focus of infection. Bar, 250 μm. (D) Extensive infection is visible in a transverse section through the nasal cavity. The directions of the inhaled and exhaled airflow are indicated by blue and red arrows, respectively, and a schematic (inset) indicates the anatomical location of the transverse section. AD, adenoid; HP, hard palate; NC, nasal concha; NM, nasal mucosa; NP, nasopharynx; SP, soft palate. (E) Direct detection of a focus of EGFP-positive cells on the surface of the nasal concha. No cell-to-cell fusion was observed between MV-infected cells. Bar, 100 μm.

cheal epithelium, no positive immunostaining was observed in nonciliated basal epithelial cells present in lower levels of the epithelium. Although cell-to-cell fusion was observed in large foci of MV-infected epithelial cells, as evidenced by some degree of clustering of the nuclei (Fig. 5G), limited immune cell infiltration or disruption of the epithelium was apparent.

DISCUSSION

In contrast to infections caused by respiratory pathogens such as HRSV, seasonal influenza virus strains, and rhinoviruses, MV spreads systemically and infection of respiratory tract tissues occurs predominantly in the late stages of the disease. The identification of MV-infected cells or tissues in the URT and LRT of infected individuals contributing to MV transmission has historically proven difficult to assess, due to a paucity of published pathological studies from human measles cases which made use of a set of diverse tissue blocks free of complications caused by underlying disease or secondary bacterial infections. With the macaque being an established natural model of measles, we undertook a comprehensive analysis of the respiratory tract of MV-infected macaques to analyze the mechanism through which MV spreads into respiratory epithelium in the late stages of the disease, complementing our studies into early events in measles pathogenesis (9). The availability of tissue blocks from the respiratory tract of a large number of MV-infected animals ($n = 40$) adds weight to the conclusions from this study.

Analysis of respiratory tract tissues from MV-infected macaques highlighted the crucial role of MV-infected immune cells in the spread of virus to epithelial cells. Although long assumed, this is the first evidence of immune cells having a direct role in the spread of MV into epithelia *in vivo* and thus completes a missing link in our understanding of measles pathogenesis. A recent study also proposed a role for myeloid cells in the lamina propria of the trachea in spreading virus to the epithelium (18). However, MV-infected lymphocytes were not detected within epithelium and dual-labeling immunofluorescence stains were not performed. The *in vitro* model we have developed will be invaluable for others in understanding the importance of cell-to-cell transmission of paramyxoviruses. MV spread into epithelia is most likely mediated via the interaction of MV glycoprotein complexes on the surface of immune cells with PVRL4, which we show to be present in epithelial cell adherens junction in a wide array of tissues, including lung, bronchi, trachea, and nasal concha. This provides a mechanism through which MV can access a cellular receptor that is inaccessible to virus present in the lumen of the respiratory tract, due to its spatial localization within epithelia, and allows MV infection of epithelial cells in tissues of both the LRT and URT. Interestingly, polarized expression of PVRL4 was observed along the basolateral surface of pseudostratified ciliated epithelial cells in the trachea and nasal concha. The fact that MV infection is primarily restricted to nondividing (Ki-67-negative) pseudostratified columnar ciliated epithelial cells in tracheal epithelium, despite high levels of PVRL4 expression in dividing (Ki-67-positive) basal epithelial cells, suggests that additional host factors or the context through which such cells are contacted by MV-infected immune cells may influence the susceptibility of tracheal epithelial cells to MV infection.

We have previously reported the utility of rMV expressing fluorescent proteins to monitor virus cell-to-cell spread sensitively *in vitro* in both neural and primary epithelial cells (5, 19). In this study, we have applied these techniques to a novel *in vitro* coculture model and show rapid virus spread from MV-infected B cells to adjacent primary differentiated bronchial epithelial cells in which the adherens junctions were rendered accessible by cell wounding. This proves that immune cells are capable of transferring MV infectivity into respiratory epithelium. The key role of PVRL4 in governing MV cell-to-cell spread from immune cells to epithelial cells in this model is highlighted by the fact that an rMV strain unable to bind to PVRL4 was restricted to B-LCL. The location of PVRL4 at adherens cell junctions of epithelial cells means that this molecule is inaccessible to cell-free virus present at the apical side. Thus, we propose that MV infection of epithelial cells

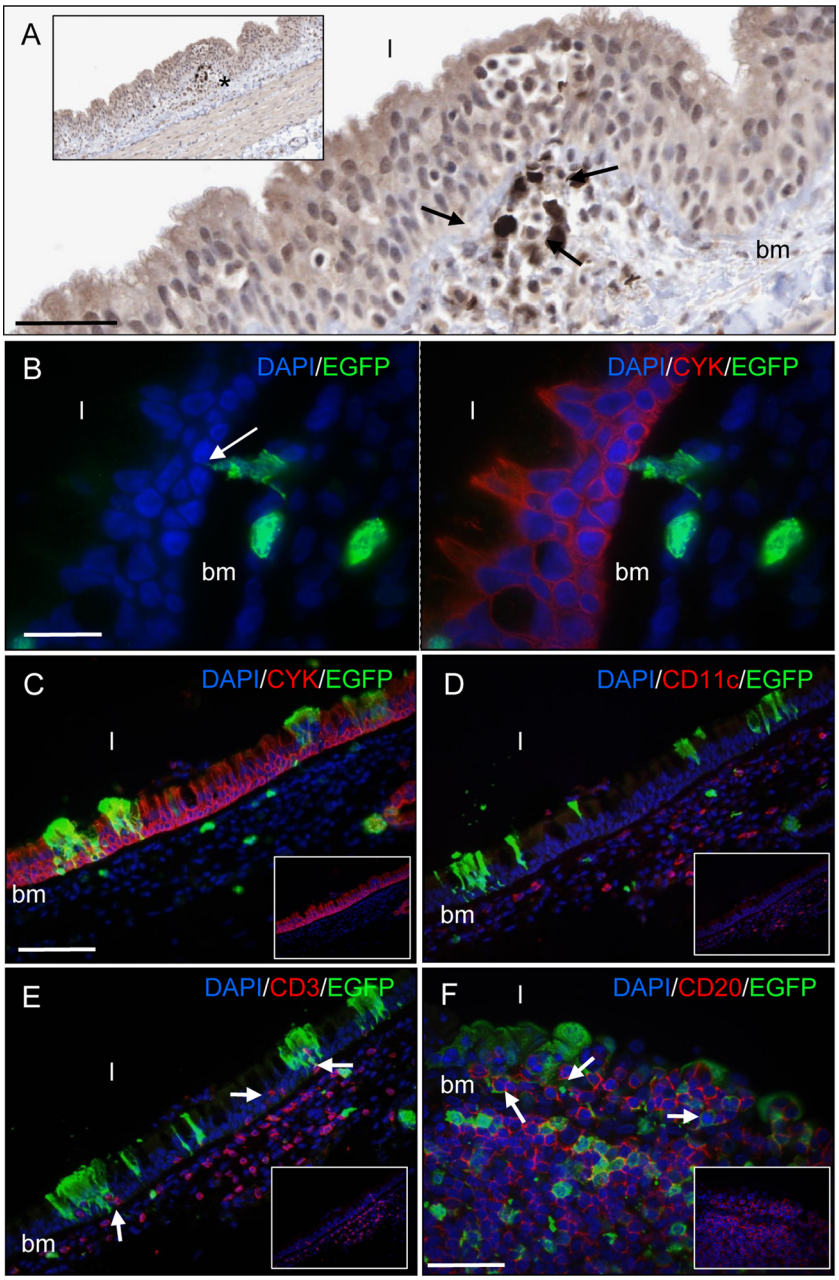

FIG 4 Detection of MV-infected and uninfected immune cells in tracheal (A to E) and bronchial (F) epithelium. Shown is immunohistochemical (A) and indirect immunocytochemical (B to F) staining of formalin-fixed tissue sections taken from infected macaques at 7 d.p.i., prior to the peak of infection (A and B), and at the peak of infection at 9 d.p.i. (C to F). MV-infected cells were detected with a polyclonal anti-EGFP antibody. (A) MV-infected leukocytes observed beneath tracheal epithelium. Bar, 40 μm. (Inset) Lower-magnification image of the main panel; the location of the infected cells highlighted with an asterisk. bm, basement membrane; l, lumen. (B) A cellular process from an MV-infected myeloid cell (green) interdigitating between cytokeratin-positive pseudostratified columnar epithelial cells (red). Bar, 20 μm. (C) Colocalization is observed between EGFP (green) and cytokeratin-positive epithelial cells (red). (D) CD11c-positive myeloid cells (red) are present in the lamina propria. (E) Infiltration of CD3-expressing T cells (red) (arrows) into regions of epithelium containing foci of MV-infected epithelial cells (green). Bar (C to E), 100 μm. (F) Infiltration of uninfected and infected CD20-positive B cells (red) (arrows) into bronchial epithelium from an underlying aggregate of lymphoid tissue. Bar, 50 μm. DAPI was used to counterstain cell nuclei (blue).

primarily occurs via cell-to-cell fusion between resident or infiltrating MV-infected immune cells and PVRL4$^+$ epithelial cells rather than virus-to-cell fusion. Further research is required using model systems in which PVRL4 is expressed in its normal architectural location rather than overexpression in continuous cell lines in order to gain a more complete understanding of the differences between these two modes of virus spread and ultimately their relevance to virus spread *in vivo*.

Recently, the trachea has been proposed as the primary site from which MV emerges into the airways of the respiratory tract prior to transmission to a susceptible host (8, 20). However, our analysis of MV infection and related pathology of respiratory tract

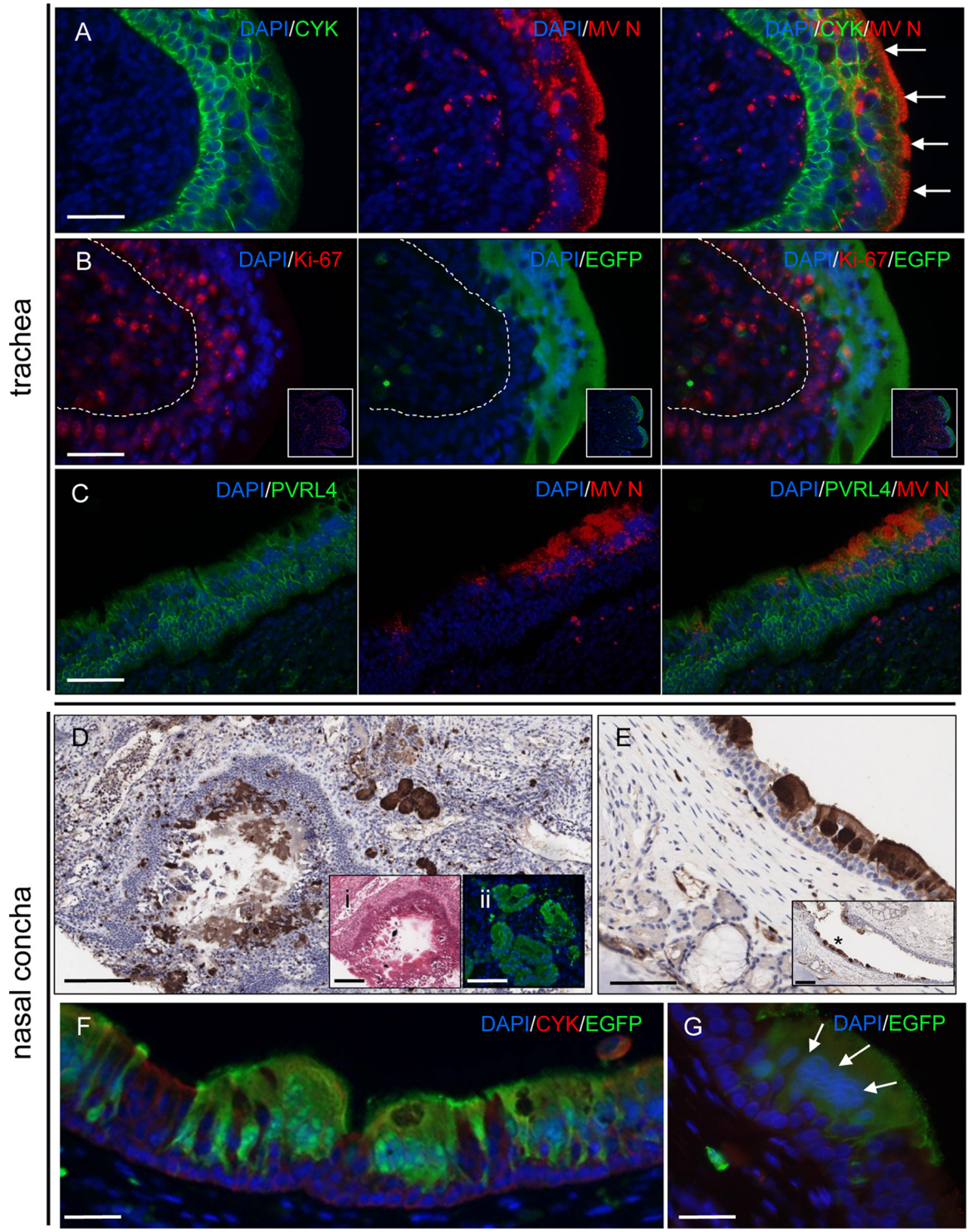

FIG 5 Detection of MV-infected cells in the trachea and nasal epithelium. (A) Dual labeling of cytokeratin (green) and MV N (red) showing MV infection of the luminal epithelial cell layers. MV N was observed to accumulate beneath the apical cell membrane (arrows). Bar, 50 μm. (B) MV does not infect proliferating basal epithelial cells in the trachea. Little colocalization is observed between EGFP (green) and Ki-67 (red), a marker of cell proliferation. The approximate location of the division between the epithelium and the subepithelial cell layers is shown by a dashed line. Bar, 50 μm. (Insets) Lower-magnification images of main panels showing localized expression of Ki-67. (C) No alteration of PVRL4 expression (green) is visible within a large focus of MV-infected cells (red) in the trachea. Bar, 80 μm. (D) Large numbers of MV-infected epithelial cells are present in an immunohistochemically stained section of nasal concha. Bar, 160 μm. (Inset i) H&E-stained serial section of nasal concha showing shedding of epithelial cells into the lumen. Bar, 160 μm. (Inset ii) Serial section of nasal concha showing immunofluorescence detection of EGFP in adjacent epithelial cells. Bar, 100 μm. (E) Immunohistochemical detection of EGFP in epithelial cells in URT epithelium. Bar, 80 μm. (Inset) Lower magnification of MV-infected epithelial cells (asterisk) shown in the main panel. Little infection is apparent in the basal epithelial cell layers of the epithelium. Bar, 160 μm. (F) Dual labeling of EGFP (green) and cytokeratin-positive pseudostratified columnar epithelial cells (red) in URT epithelium. Bar, 50 μm. (G) Cell-to-cell fusion of MV-infected epithelial cells (green) in a large focus of infection in URT epithelium results in clustering of cell nuclei (arrows). Bar, 30 μm. Nuclei were visualized using DAPI (blue).

epithelia presents a more complex picture. While we detected large circular foci of MV-infected ciliated epithelial cells along the inner surface of the trachea, the overall burdens of MV infection and associated lesions were lower than those of the nasal concha and mucosa in the nasal cavity, in which strong PVRL4 expression in epithelia was also observed. The anatomical location of these tissues means that virus shed from these sites is inherently more likely to be expelled into the environment by airflow than virus emerging lower in the airways, which has to survive neutralization for a longer time period by host factors present in mucus and saliva. A number of other viruses transmitted via the respiratory route are known to infect the URT, including HRSV, coronaviruses, and rhinoviruses (21–23). In the case of Sendai virus, transmission of virus from infected animals was directly associated with infection of the URT and was independent of infection in the lung (24). Conversely, H5N1 strains of influenza cause significant disease in humans with high case fatality rates, but usually remain restricted to the initial index patient due to the fact that the virus replicates mostly in the LRT (25, 26). While the cough reflex typically associated with measles is triggered by stimulation of sensory nerves at or below the level of the larynx, URT infections can also trigger a productive cough due to nonspecific effects of inflammatory mediators and increased mucus production on sensory nerve endings in the bronchi and trachea in the LRT (22).

In summary, we propose a mechanism for the introduction of MV into the respiratory epithelium following viremia, via the infiltration of MV-infected immune cells and subsequent spread to PVRL4-positive pseudostratified columnar epithelium, and demonstrate an analogous mode of cell-to-cell spread in a novel *in vitro* coculture model of respiratory epithelium. Differential levels of MV infection were observed in epithelium from different respiratory tract tissues, with nasal epithelium in the URT consistently displaying a high level of infection. This emerging view of the late stages of measles pathogenesis should lead to further experiments focused on the aerosolized transmission of morbilliviruses.

ACKNOWLEDGMENTS

We thank the staff of the Tissue Core Technology Unit and the Bioimaging Unit, QUB, for expert technical assistance, Yusuke Yanagi for providing the Vero-hCD150 and A549-hCD150 cell lines and the plasmid from which the rMV^{IC323}EGFP virus was rescued, and Thijs Kuiken and Bert Rima for helpful discussions. In addition, we thank Robert Dias D'Ullois, Tien Nguyen, and Linda Rennick for their contributions to these studies.

This work was funded by MRC grant no. G0801001 and ZonMw grant no. 91208012.

The funding agencies had no role in study design, data collection, and analysis or the decision to publish or preparation of the manuscript.

REFERENCES

1. **Moss WJ, Griffin DE.** 2006. Global measles elimination. Nat. Rev. Microbiol. **4**:900–908.
2. **ECDC.** 21 February 2012. Surveillance report. European monthly measles monitoring (EMMO). Issue 8. European Centre for Disease Prevention and Control, Stockholm, Sweden. http://ecdc.europa.eu/en/publications/publications/sur_emmo_European-monthly-measles-monitoring-february-2012.pdf.
3. **Simons E, Ferrari M, Fricks J, Wannemuehler K, Anand A, Burton A, Strebel P.** 2012. Assessment of the 2010 global measles mortality reduction goal: results from a model of surveillance data. Lancet **379**:2173–2178.
4. **Tahara M, Takeda M, Shirogane Y, Hashiguchi T, Ohno S, Yanagi Y.** 2008. Measles virus infects both polarized epithelial and immune cells by using distinctive receptor-binding sites on its hemagglutinin. J. Virol. **82**:4630–4637.
5. **Ludlow M, Rennick LJ, Sarlang S, Skibinski G, McQuaid S, Moore T, de Swart RL, Duprex WP.** 2010. Wild-type measles virus infection of primary epithelial cells occurs via the basolateral surface without syncytium formation or release of infectious virus. J. Gen. Virol. **91**:971–979.
6. **Leonard VH, Sinn PL, Hodge G, Miest T, Devaux P, Oezguen N, Braun W, McCray PB, McChesney MB, Cattaneo R.** 2008. Measles virus blind to its epithelial cell receptor remains virulent in rhesus monkeys but cannot cross the airway epithelium and is not shed. J. Clin. Invest. **118**:2448–2458.
7. **Noyce RS, Bondre DG, Ha MN, Lin LT, Sisson G, Tsao MS, Richardson CD.** 2011. Tumor cell marker PVRL4 (nectin 4) is an epithelial cell receptor for measles virus. PLoS Pathog. **7**:e1002240. doi:10.1371/journal.ppat.1002240.
8. **Muhlebach MD, Mateo M, Sinn PL, Prufer S, Uhlig KM, Leonard VH, Navaratnarajah CK, Frenzke M, Wong XX, Sawatsky B, Ramachandran S, McCray PB, Cichutek K, von Messling V, Lopez M, Cattaneo R.** 2011. Adherens junction protein nectin-4 is the epithelial receptor for measles virus. Nature **480**:530–533.
9. **Lemon K, de Vries RD, Mesman AW, McQuaid S, van Amerongen G, Yuksel S, Ludlow M, Rennick LJ, Kuiken T, Rima BK, Geijtenbeek TB, Osterhaus AD, Duprex WP, de Swart RL.** 2011. Early target cells of measles virus after aerosol infection of non-human primates. PLoS Pathog. **7**:e1001263. doi:10.1371/journal.ppat.1001263.
10. **de Swart RL, Ludlow M, de Witte L, Yanagi Y, van Amerongen G, McQuaid S, Yuksel S, Geijtenbeek TB, Duprex WP, Osterhaus AD.** 2007. Predominant infection of CD150+ lymphocytes and dendritic cells during measles virus infection of macaques. PLoS Pathog. **3**:e178. doi:10.1371/journal.ppat.0030178.
11. **Mesman AW, de Vries RD, McQuaid S, Duprex WP, de Swart RL, Geijtenbeek TB.** 2012. A prominent role for DC-SIGN+ dendritic cells in initiation and dissemination of measles virus infection in non-human primates. PLoS One **7**:e49573. doi:10.1371/journal.pone.0049573.
12. **de Vries RD, McQuaid S, van Amerongen G, Yuksel S, Verburgh RJ, Osterhaus AD, Duprex WP, de Swart RL.** 2012. Measles immune suppression: lessons from the macaque model. PLoS Pathog. **8**:e1002885. doi:10.1371/journal.ppat.1002885.
13. **de Vries RD, Lemon K, Ludlow M, McQuaid S, Yuksel S, van Amerongen G, Rennick LJ, Rima BK, Osterhaus AD, de Swart RL, Duprex WP.** 2010. In vivo tropism of attenuated and pathogenic measles virus expressing green fluorescent protein in macaques. J. Virol. **84**:4714–4724.
14. **Reed LJ, Muench H.** 1938. A simple method of estimating fifty percent endpoints. Am. J. Hyg. (Lond.) **27**:493–497.
15. **Verkaik NJ, Nguyen DT, de Vogel CP, Moll HA, Verbrugh HA, Jaddoe VW, Hofman A, van Wamel WJ, van den Hoogen BG, Buijs-Offerman RM, Ludlow M, de Witte L, Osterhaus AD, van Belkum A, de Swart RL.** 2011. Streptococcus pneumoniae exposure is associated with human metapneumovirus seroconversion and increased susceptibility to in vitro HMPV infection. Clin. Microbiol. Infect. **17**:1840–1844.
16. **Takeda M, Takeuchi K, Miyajima N, Kobune F, Ami Y, Nagata N, Suzaki Y, Nagai Y, Tashiro M.** 2000. Recovery of pathogenic measles virus from cloned cDNA. J. Virol. **74**:6643–6647.
17. **Takeda M, Tahara M, Hashiguchi T, Sato TA, Jinnouchi F, Ueki S, Ohno S, Yanagi Y.** 2007. A human lung carcinoma cell line supports efficient measles virus growth and syncytium formation via a SLAM- and CD46-independent mechanism. J. Virol. **81**:12091–12096.
18. **Frenzke M, Sawatsky B, Wong XX, Delpeut S, Mateo M, Cattaneo R, von Messling V.** 19 December 2012. Nectin-4 dependent measles virus spread to the cynomolgus monkey tracheal epithelium: role of infected immune cells infiltrating the lamina propria. J. Virol. [Epub ahead of print.] doi:10.1128/JVI.03037-12.
19. **Duprex WP, McQuaid S, Hangartner L, Billeter MA, Rima BK.** 1999. Observation of measles virus cell-to-cell spread in astrocytoma cells by using a green fluorescent protein-expressing recombinant virus. J. Virol. **73**:9568–9575.
20. **Racaniello V.** 2011. Virology. An exit strategy for measles virus. Science **334**:1650–1651.
21. **Hall CB, Douglas RG, Jr, Schnabel KC, Geiman JM.** 1981. Infectivity of respiratory syncytial virus by various routes of inoculation. Infect. Immun. **33**:779–783.
22. **Eccles R.** 2005. Understanding the symptoms of the common cold and influenza. Lancet Infect. Dis. **5**:718–725.
23. **Lu R, Yu X, Wang W, Duan X, Zhang L, Zhou W, Xu J, Xu L, Hu Q,**

Lu J, Ruan L, Wang Z, Tan W. 2012. Characterization of human coronavirus etiology in Chinese adults with acute upper respiratory tract infection by real-time RT-PCR assays. PLoS One **7**:e38638. doi:10.1371/journal.pone.0038638.

24. **Burke CW, Mason JN, Surman SL, Jones BG, Dalloneau E, Hurwitz JL, Russell CJ.** 2011. Illumination of parainfluenza virus infection and transmission in living animals reveals a tissue-specific dichotomy. PLoS Pathog. **7**:e1002134. doi:10.1371/journal.ppat.1002134.
25. **van Riel D, den Bakker MA, Leijten LM, Chutinimitkul S, Munster VJ, de Wit E, Rimmelzwaan GF, Fouchier RA, Osterhaus AD, Kuiken T.** 2010. Seasonal and pandemic human influenza viruses attach better to human upper respiratory tract epithelium than avian influenza viruses. Am. J. Pathol. **176**:1614–1618.
26. **van Riel D, Munster VJ, de Wit E, Rimmelzwaan GF, Fouchier RA, Osterhaus AD, Kuiken T.** 2006. H5N1 virus attachment to lower respiratory tract. Science **312**:399. doi:10.1126/science.1125548.